Available online at www.sciencedirect.com
ScienceDirect
Trans. Nonferrous Met. Soc. China 35(2025) 1−12
Transactions of Nonferrous Metals Society of China
www.tnmsc.cn

Atomic-scale insights into microscopic mechanisms of grain boundary segregation in Al−Cu alloys

Xiong SHUAI[1], Hong MAO[2], Sai TANG[3], Yi KONG[1], Yong DU[1]

1. State Key Laboratory of Powder Metallurgy, Central South University, Changsha 410083, China;
2. College of Mechanical Engineering, Hunan Institute of Science and Technology, Yueyang 414006, China;
3. National Key Laboratory of Science and Technology on High-strength Structural Materials, Central South University, Changsha 410083, China

Received 5 June 2023; accepted 26 September 2023

Abstract: This study aims to clarify the mechanisms for the grain boundary (GB) segregation through investigating the absorption of excess solute atoms at GBs in Al−Cu alloys by using the hybrid molecular dynamics/Monte Carlo simulations. Two segregation mechanisms, substitutional and interstitial mechanisms, are observed. The intergranular defects, including dislocations, steps and vacancies, and the intervals in structural units are conductive to the prevalence of interstitial mechanism. And substitutional mechanism is favored by the highly ordered twin GBs. Furthermore, the two mechanisms affect the GB structure differently. It is quantified that interstitial mechanism is less destructive to GB structure than substitutional one, and often leads to a segregation level being up to about 6 times higher than the latter. These findings contribute to atomic scale insights into the microscopic mechanisms about how solute atoms are absorbed by GB structures, and clarify the correlation among intergranular structures, segregation mechanisms and kinetics.

Key words: grain boundaries segregation; Al−Cu alloy; intergranular structure; molecular dynamics simulation; Monte Carlo simulation

1 Introduction

Grain boundary (GB) segregation is a ubiquitous phenomenon in polycrystalline materials during which excess solute atoms, driven by GB energy reduction, move toward GBs from the bulk of grains. This often leads to solute enrichment at GBs with an amazing level exceeding the concentration in the bulk of grains by 2−3 times and sometimes even by up to several orders of magnitude [1]. Such a dramatic change in chemical composition around the GB could be essentially attributed to the imperfections of the GB structure. In reverse, researchers have found that solute enrichment may bring significant changes to GB behaviors and ultimately to the properties of materials [2−6]. On the one hand, detrimental effects might be brought. The enrichment of Cu atoms at GBs significantly changes the chemical composition around GB and may induce GB precipitation, which substantially undermines the plasticity and corrosion resistance of the Al−Cu alloys [7,8]. On the other hand, GB segregation has been employed as an important strategy to improve materials properties and design new materials [9−11]. This can increase the thermodynamic stability of nanoscale polycrystalline materials, inhibiting the

Corresponding author: Sai TANG, Tel: +86-731-88877825, E-mail: s.tang@csu.edu.cn;
Yong DU, Tel: +86-731-88877300, E-mail: yong-du@csu.edu.cn
https://doi.org/10.1016/S1003-6326(24)66661-6
1003-6326/© 2025 The Nonferrous Metals Society of China. Published by Elsevier Ltd & Science Press
This is an open access article under the CC BY-NC-ND license (http://creativecommons.org/licenses/by-nc-nd/4.0/)

coarsening of nanograins [12]. Therefore, GB segregation has aroused great interests from the community of materials science in the last decades [13−15].

Unraveling the interactions between solute atoms and GB structure is the key to understand the physical mechanisms of GB segregation. Essentially, GB segregation is determined by GB intergranular structures, including dislocations, vacancies, small steps, structural units (ordered arrangement of small atom groups, often showing polyhedral shape), and so on [16,17]. Since GB segregation is confined to the narrow GB region with a width of the nanoscale, it is conceivable that such intergranular structures are responsible for absorbing and accommodating segregated atoms. Theoretically, the analytical models such as Gibbs Adsorption Isotherm, Langmuir−Mclean Isotherm, and GB density model have established the thermodynamic correlations between the solute segregation level and GB features [18−21]. These theoretical models have verified the influences of GB properties on solute segregation, providing us valuable approaches to estimate GB segregation. However, neglecting the atomic-scale information of GB structure, they failed to capture the interaction between the adsorption of solute atoms and GB structures. By combining transmission electron microscopy (TEM) characterization with atom probe tomography (APT) measurement, experimental studies have quantified the distribution of enriched solute atoms in GBs as well as the relationship between GB misorientation and solute enrichment [22−24]. Nevertheless, it is still technically challenging to explain the mechanisms about how the intergranular structures absorb excess solute atoms through experimental characterizations. This prevents us from a microscopic view of the mechanism of solute segregation in GBs. Specifically, we need to know how the intergranular structures interact with foreign solute atoms, and more importantly, where the segregated atoms are.

In this study, by using the hybrid molecular dynamic (MD)/Monte Carlo (MC) method [25,26], we contrive to address the fundamental problem how GBs absorb and accommodate enriched solute atoms on the atomic scale. The hybrid MD/MC simulations have shown the potential to study the microscopic mechanisms of structural and compositional evolution for phase transformations and chemical reactions. However, these researches mainly focused on the interaction among different components. An in-depth understanding on the mechanisms of the interaction between GB segregation sites and solute atoms is still lacking. Here, the hybrid MD/MC simulation is employed to study this issue in Al−Cu binary alloys. The significance of this study is that it clarifies both the atomic scale physics of structural and compositional evolutions in GB segregation on the atomic scale. This work enhances our understanding on the fundamental issues of GB segregation, such as how GB segregation proceeds and the intimate correlations among GB structure, GB segregation mechanism and the kinetics of GB segregation.

2 Method and simulation details

The hybrid MD/MC simulations are performed using the large-scale atomic/molecular massively parallel simulator (LAMMPS) program [27]. As shown in Fig. 1(a), Cu atoms entering into the matrix are resulted from the combined action of MD and MC steps, rather than additional artificial manipulation. The MD steps are responsible for equilibrating atoms. Based on the variation of free energy, the MC step could delete or insert atoms, exchange atom positions, and decide whether or not to add a Cu atom at a site. Combining the MD and MC steps by suitable potential function, we could describe the process of solute segregation.

The embedded-atom method (EAM) potentials for the Al−Cu system developed by LIU et al [28] are adopted in our simulations. The integration time step for MD simulations is 1 fs. The initial GB samples are first equilibrated to the minimum potential energy state using a conjugate gradient minimization technique and then are relaxed with a Nose–Hoover thermo/barostat for 20 ps under zero pressure at 100 K [29].

A variance-constrained semi-grand canonical ensemble (VC-SGC) is used to perform MC steps [30]. In a system that N particles are confined within a box of volume V at temperature T, each particle carries a spin value of 0 or 1. The partition function (Z_V) of the VC-SGC ensemble in terms of the canonical one is expressed as

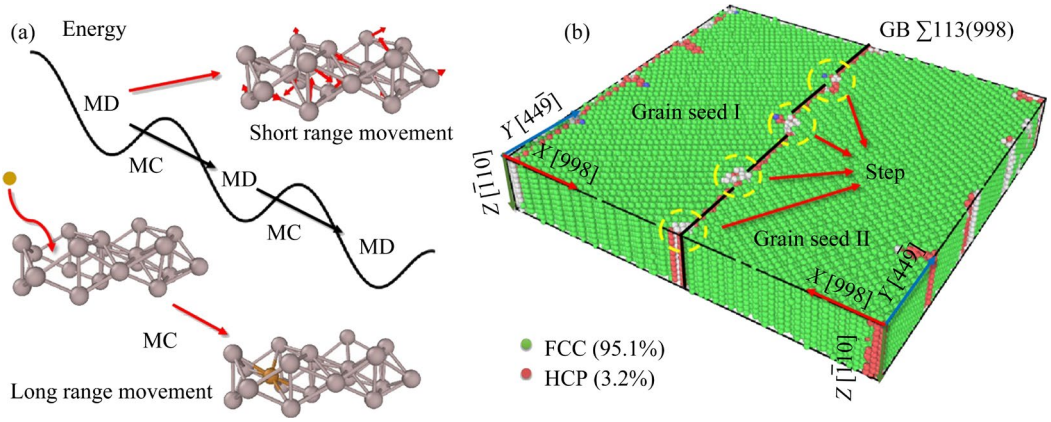

Fig. 1 Sketch of operating mode for MD/MC hybrid simulation (a), and construction of atomic configuration of initial GB Σ113(998) in simulation (b)

$$Z_{\mathrm{V}}(\phi,\kappa,\Lambda)=\int_0^1 Z_{\mathrm{C}}(c,\Lambda)\exp\left[-\beta Nc(\phi+\kappa Nc)\right]\mathrm{d}c \tag{1}$$

where $\Lambda=\{N,V,T\}$ is the set of independent thermodynamic variables [30], Lagrange multipliers ϕ and κ are related to constraints on the first and the second moments of the concentration respectively, c is the solute concentration, Z_{C} is the partition function for the canonical ensemble, and $\beta=1/(k_{\mathrm{B}}T)$. The reservoir of the VC-SGC ensemble is controlled by two independent parameters, ϕ and κ. Compared with the SGC ensemble, the VC-SGC ensemble is more suitable to study equilibrium properties of multiphase systems [30]. In addition, the MC algorithm for sampling the VC-SGC ensemble is very similar to that of the SGC ensemble. For more details about the MC simulation with VC-SGC ensemble and the related MC algorithm, readers could refer to Refs. [30,31]. In the MC steps, κ=1000 and the initial chemical potential is set as 1 [30].

In the MD/MC steps, a Nose–Hoover thermo/barostat with zero pressure at 500 K is used, and MC step switches occur after every 10 or 100 MD steps, with the global concentration fixed to be 1.1 at.% Cu by adjusting the chemical potential difference during the simulation. A MC step is followed by relaxation in an NPT (Number−Pressure−Temperature) ensemble for 0.1 ps under zero pressure at a given temperature. This procedure would be repeated until the equilibrium configuration is reached. The simulation stops when the absolute value of the slope of the potential energy over the last 400 ps of MD simulation is less than 1 eV/ps. After equilibration and cooling, each system is relaxed at 100 K for an additional 150 ps. For statistical purposes, six thermodynamically equivalent configurations of each system are stored (every 10 ps) during the last 50 ps of the equilibration process.

In this work, four ⟨110⟩ symmetric tilt GBs, the twin GB Σ3(111), Σ113(998) (the vicinal GB to the twin GB), Σ19(331) (a normal high angle tilt GB), and Σ201(11,20) (a low angle tilt GB), are selected. As shown in Fig. 1(b), being similar to pure MD simulations, the initial atom configuration of GB Σ113(998) is constructed by ATOMSK [31]. The simulation box is approximately 18 nm in length, 18 nm in width, and 3−4 nm in thickness, and contains about 50000 atoms. It should be noted that the specific size of the samples for different GBs may be slightly different. As shown in Fig. 1(b), the GB Σ113(998) with length of 18 nm contains four intergranular steps. Besides, within the same GB length, there are nine intergranular dislocations in GB Σ201(11,20), and even more structural units in GB Σ3(111) and GB Σ19(331). The number of discrete intergranular structures contained in the four GBs with a length of 18 nm is geometrically sufficient for the periodic boundary condition. The concentrations for all the simulation samples are set as Al−1.1at.%Cu. The atomic configurations are visualized by using the open-source visualization tool OVITO [32].

3 Result and discussion

3.1 Grain boundary structure characterization

Figure 2 shows the GB energy and GB density

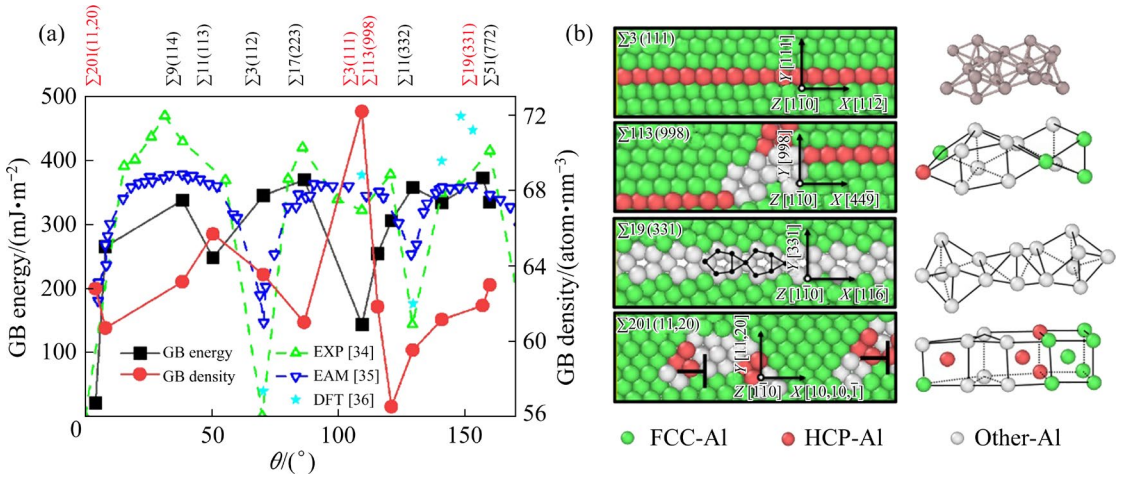

Fig. 2 GB energy and GB atom number density as function of tilt angle (θ) for ⟨110⟩ tilt GBs (a), and atomic configurations of relaxed Σ3(111), Σ113(998), Σ19(331) and Σ201(11,20) GBs (b)

(atom number density) [33] of ⟨110⟩ tilt GBs for pure Al, as well as the atomic configurations of four selected ⟨110⟩ symmetric tilt GBs. The GB density ρ_{GB} (GB atom number density), i.e., the total number of atoms per unit volume near the grain boundary, is calculated as $\rho_{GB}=N_{total}/V_{GB}$, where N_{total} is the total number of atoms in the thin slab (with a thickness of 0.6 nm) around GB plane, and V_{GB} is the volume of the thin slab. Essentially, the GB density is thermodynamically related to GB energy, and is thermodynamically consistent with the GB excess free volume in measuring the GB properties [6]. Besides, the variation of GB concentration and structure caused by solute segregation can be intuitively characterized by GB density [5,6].

The values of GB energy and dependences on GB misorientation (θ) calculated in this work agree well with previous experimental [34], EAM [35] and DFT [36] results. Two local minimum values of GB energy correspond respectively to the twin GB Σ3(111) and the GB Σ11(113). The change of GB density with the misorientation (θ) shows generally an opposite trend with the variation of GB energy with θ except the range from 120° to 160°, and two maxima of GB density also correspond respectively to the twin GB Σ3(111) and the GB Σ11(113). The opposite trend has also been found in previous studies [6,33]. In addition, the conflict of the opposite trend when θ ranges from 120° to 160° may probably be caused by the errors of the MD/MC calculations. In fact, the experimental and EAM results in Fig. 2(a) show that the GB density increases monotonically with θ ranging from 120° to 160°.

The atomic configurations of the intergranular structures in the four selected GBs are investigated, as shown in Fig. 2(b). Here, GB density and GB energy are used to describe GB structures. The GB density is calculated through dividing the total number of atoms along the GB with a width of 0.6 nm by the corresponding volume. The twin GB Σ3(111) is composed of a periodic arrangement of a single structural unit, which can be classified as the first level according to PAIDAR's hierarchical classification [37]. The Σ113(998) GB is generated by rotating the abutting grains of the twin GB Σ3(111) with a small angle of 3.1°. Its intergranular structure is nearly the same as that of the twin GB Σ3(111), except periodically distributed small steps along the ⟨110⟩ direction. The steps lead to a steep increase in the GB energy and a steep decrease in the GB density compared with twin GB Σ3(111). As a general high angle GB, GB Σ19(331) is constituted by two types of structural units arranged periodically and alternately. Besides, the low angle tilt GB Σ201(11,20) with a misorientation angle of 8.09° is studied. Its intergranular structure is an array of edge dislocations.

3.2 Dependence of solute segregation on GB structure

The amount of GB segregation and distribution of solute Cu atoms in GBs for an Al−1.1at.%Cu alloy is quantified, as shown in Fig. 3. The dependence of the solute concentrations

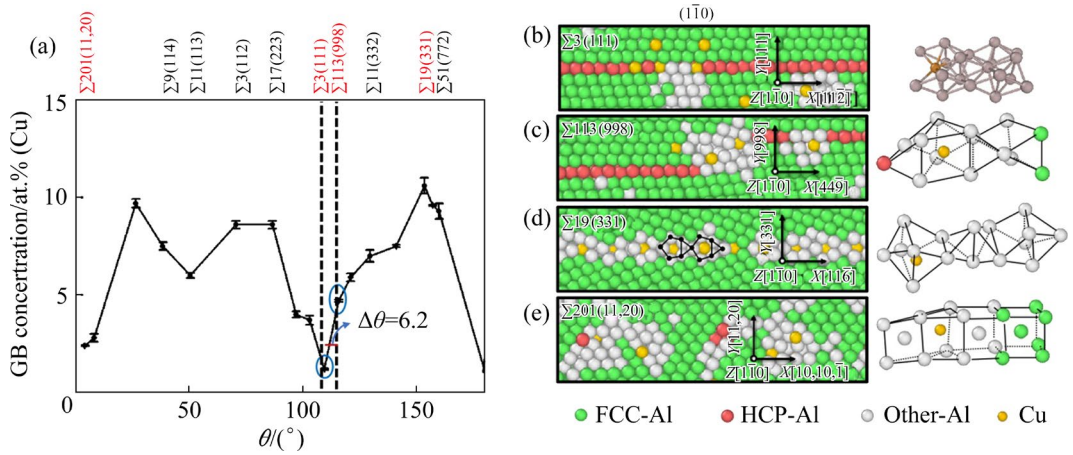

Fig. 3 GB segregation as function of misorientation angle (θ) in Al−1.1at.%Cu alloy (a), and atomic snapshots of GBs Σ3(111) (b), Σ113(998) (c), Σ19(331) (d), and Σ201(11,20) (e) after segregation

in GBs on the misorientation angle (θ) of the tilt ⟨110⟩ GBs is very similar to that of the GB energies. Being similar to the GB energy, two minima at the twin GB Σ3(111) and the GB Σ11(113) are observed. In particular, the solute concentration at Σ3(111) GB is approximately 1.1 at.% Cu, which is basically the same as that in the matrix phase. Such a low amount of segregation suggests that the twin GB is disadvantageous to absorb solute atoms from abutting grains. The atomic configuration of the twin GB with about 1.1 at.% Cu atoms in Fig. 3(b) indicates that the twin GB provides few site for foreign Cu atoms, and the segregated Cu atoms have to replace the original Al atoms via a substitution way.

However, surprisingly, the solute concentration of Σ113(998) GB increases significantly, although GB Σ113(998) deviates slightly from the twin GB by merely 3.1°. Experimental studies have also reported similar dramatic variation in the solute segregation of the vicinal GBs to the twin GB [38]. Such dependences of solute segregation on GB misorientation are in good agreement with APT quantifications [38]. Further, our simulations explain this steep variation by characterizing the distribution of solute atoms in intergranular structures on the atomic scale. The atomic-scale characterizations of the GB structure in Fig. 3(c) clearly confirm that the intergranular small steps in GB Σ113(998) are responsible for the steep increase of segregated solute atoms. The defects around the steps produce additional intervals to capture Cu atoms, as shown in the right panel of Fig. 3(c). In recent years, atomistic hybrid MD/MC simulations of solute segregation in nanocrystalline alloys have also verified that the introduction of intergranular steps in twin GBs contributes to substantial increase of solute enrichment [39−42].

For the general high angle GB Σ19(331), it is found that the segregated Cu atoms are mainly located inside the intervals of the polyhedral structural units. As shown in the right panel of Fig. 3(d), the two periodically arranged structural units provide plenty of intervals to arrest Cu atoms. This contributes to a high amount of segregation, as quantified by Fig. 3(a). In contrast, the low angle tilt GB Σ201(11,20) provides much less site to accommodate the segregated Cu atoms. As shown in Fig. 3(e), the atomic configuration for GB Σ201(11,20) demonstrates that the intervals of the cores of the discrete intergranular dislocations provide most space for Cu atoms. The solute segregation is limited by dislocation density in the GB, and thus the amount of segregation is generally lower than that of the high-angle GBs.

The results demonstrate that the intergranular nanostructures determine the amount of solute segregation, and more importantly the microscopic mechanisms for the adsorption of solute atoms into GBs. Compared with experimental studies about the dependency of segregation on GB misorientation angle (θ) [38], our simulation results unravel further the microscopic view how intergranular nanostructure accommodates segregated atoms, i.e., where the segregated atoms are.

3.3 Influence of solute segregation on GB structure

Figure 4 presents the influences of segregated

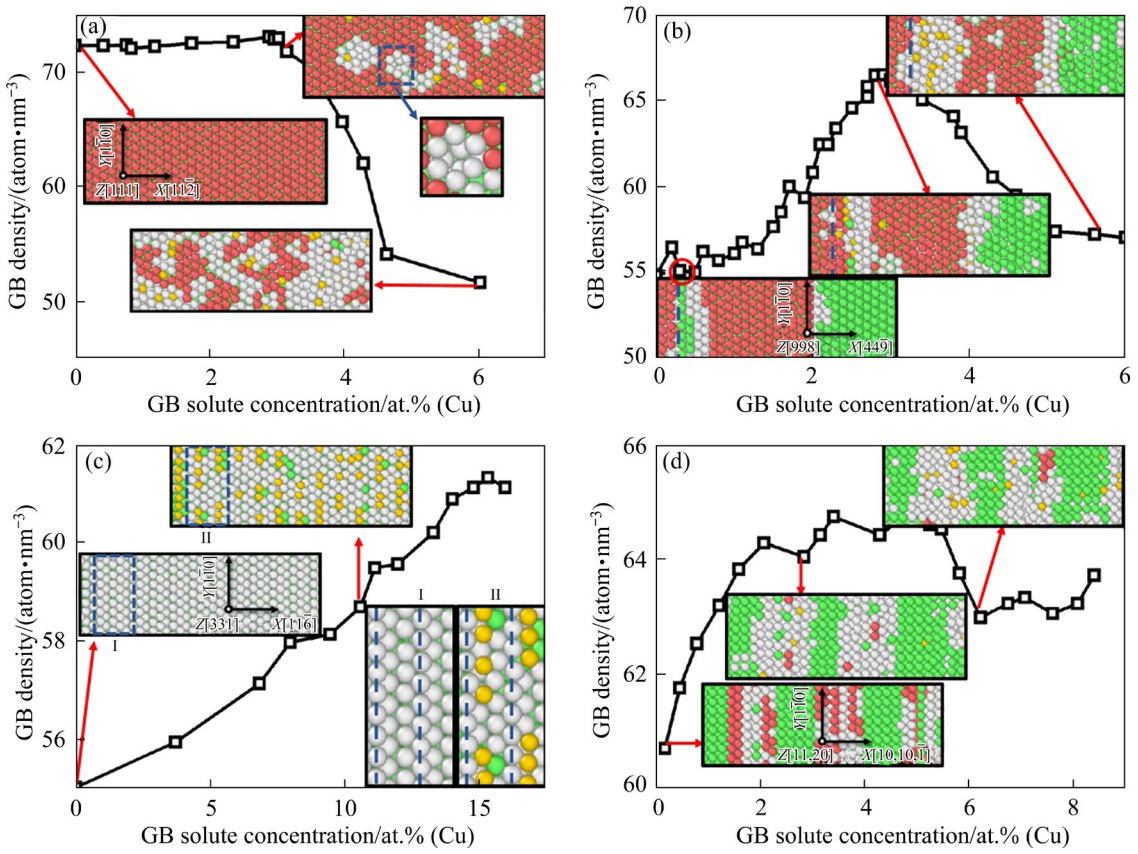

Fig. 4 GB density and atomic configuration of GB plane as function of GB segregation concentration for GB Σ3(111) (a), Σ113(998) (b), Σ19(331) (c), and Σ201(11,20) (d)

Cu atoms on the GB structure. The variation of GB structure is quantified by the variation of GB density due to the increase of solute Cu atoms. The inset figures are snapshots of the atomic configurations of GB planes at different segregation levels. Inset figures I and II in Fig. 4(c) are the enlarged views of the enclosed regions I and II in atomic snapshots of the GB plane, respectively. Theoretically, the accumulation of solute Cu atoms at GBs (C_{GB}) could increase the GB density [1]. However, an interesting phenomenon occurs at the twin GB Σ3(111). Its GB density shows a sharp downward trend with increasing Cu atoms. To explain it, we investigate the atomic configurations and the distribution of solute atoms in the GB plane ({111} plane of the fcc lattice) with different amounts of solute segregation, as shown by the inserted figures in Fig. 4(a). As the close-packed plane, the GB plane of the twin GB Σ3(111) is hard to absorb solute atoms. But its structural perfection is sensitive to segregated Cu atoms. Figure 4(a) clearly shows that the segregated Cu atoms undermine their surrounding close-packed structure in the twin GB plane. It is found that Cu atoms are segregated to the GB by substituting Al atoms. Thus, the original Al—Al bonds (about 2.86 Å) are replaced by much shorter Al—Cu bonds (about 2.53 Å), causing local strains around Cu atoms [43]. The surrounding ordered local hcp structures in the GB plane are decomposed, giving rise to vacancies and local disorder structures, as shown by the enlarged view of the dashed box in Fig. 4(a). Such non-close packed structures increase with the accumulation of Cu atoms on GBs, causing a substantial decrease in GB density.

Interestingly, the segregation of Cu atoms to the GB (Σ113(998)) is very different. As shown in Fig. 4(b) and Fig. 2, its GB plane is actually a vicinal plane to the {111} plane (the GB plane of the twin GB). It is characterized by periodically distributed {111} terraces which are separated by intergranular ⟨110⟩ steps. Though close-packed {111} terraces are disadvantageous to capture Cu atoms, the non-close packed intergranular steps containing plenty of kinks, intervals, vacancies etc., act as energetically-favored sites to accommodate

foreign Cu atoms. Almost all the segregated Cu atoms are located at the intergranular steps. The adsorption of Cu atoms to the loose steps consequently leads to an increase in the GB density when the segregation amount (concentration of segregated Cu at the GB) is less than 3 at.%. However, as the segregation amount increases, intergranular steps are gradually fulfilled by segregated Cu atoms, and finally are unable to accommodate more Cu atoms. In this circumstance, Cu atoms have to move to the close-packed {111} terraces by substituting Al atoms in the same way as solute segregation at the twin GB in Fig. 4(a). Thus, GB density decreases accordingly when the GB segregation amount is more than 3 at.%.

As shown in Fig. 4(c), for the high angle tilt GB Σ19(331), the number of intergranular ⟨110⟩ steps in its GB plane (marked by dashed lines in the inset figures) is larger than that of Σ113(998). It is clearly shown that plenty of Cu atoms are absorbed by such steps. Besides, Fig. 3(c) shows that the polyhedral intervals of structural units in GBs can also capture Cu atoms. The sufficient absorption sites of Cu atoms on this GB contribute to a higher segregation amount than twin GB and its vicinal GB Σ113(998). Obviously, the absorption of Cu atoms into steps and the intervals of structural units increase the GB density.

At the low-angle GB, Cu atoms are mainly concentrated around the dislocation cores, as shown in Fig. 4(d). Polyhedral intervals around the dislocations are characterized by Fig. 2 and Fig. 3(b), and the vacancies around dislocation cores can absorb Cu atoms. This results in a substantial increase in GB density when the GB segregation amount is less than 2 at.%. However, as the amount of Cu atoms increases, the dislocations core cannot accommodate more Cu atoms, and Cu atoms are segregated to GBs in a substitutional way like the twin GB also, making the GB density decrease when the Cu concentration is higher than 5 at.%.

Moreover, band orientation order $Q6$ [44,45] is employed to quantify the structural order of the GB region within a slice of 1.4 nm in thickness. $Q6$ has been used to identify atoms with various local structures. Usually, $0.554<Q6<0.594$ represents the fcc structure, and the farther away from this value, the lower the order of the structure [46]. As more and more Cu atoms are segregated to GBs, the order of GB decreases and converges gradually, implying a change in the GB structure. Among the four GBs, the twin GB with the highest order ($Q6$=0.517), decreases most steeply and becomes the most disordered one even with a very low GB concentration of 2 at.%, as shown in Fig. 5. As discussed above, the accumulated local strain resulting from substitutional Cu atoms in the twin GB could significantly undermine rigid twin GB, and lead to the formation of a disordered structure. For the Σ201(11,20) with a slightly lower structural order, its order decreases at a smaller rate than the twin GB, but much faster than GBs Σ19(331) and Σ113(998). The results indicate that the GB with a higher order is more susceptible to being undermined by the segregated atoms.

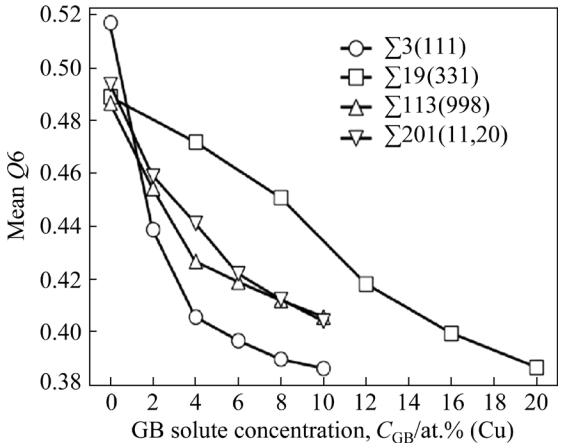

Fig. 5 Dependence of mean band orientation order ($Q6$) on GB solute concentration (C_{GB}) at different GBs

In contrast, although the normal GB Σ19(331) presents a much lower crystal order with $Q6$=0.485, its order decreases much more gently as GB concentration increases. This is because the GB Σ19(331) is a loose structure with plenty of intervals to accommodate solute atoms, thus owning a higher tolerance for the amount of segregation. As a result, the GB Σ19(331) exhibits the highest structural order after solute segregation. By comparing the $Q6$ evolution of GB Σ19(331) with that of the twin GB, it is demonstrated that the change of GB structure with solute segregation is related to the segregation mechanism. Solute atoms absorbed by intervals undermine GB structure order less than solute atoms segregated by the substitutional mechanism.

3.4 Atomic scale mechanisms of GB segregation

Two atomic mechanisms for GB segregation are found: (1) Substitutional segregation, during which Al atoms are replaced by solute atoms; (2) Interstitial segregation, during which solute Cu atoms are inserted into the kinks, vacancies, and intervals inside GBs. The substitutional segregation dominates when there are very limited energetically-favored sites accommodating foreign solute atoms, e.g., the twin GB, some special coincidence site lattice GBs, and low angle tilt GBs. As shown in Fig. 6(a), the substitutional segregation could proceed through two steps: first, an Al atom is squeezed out and replaced by a vacancy, and second, the vacancy is filled by segregated Cu atoms. In contrast, interstitial segregation prevails when there are plenty of adsorption sites in GBs, especially small steps and structural units with large intervals. The interval of the structure units in Σ19(331) in Fig. 6(b) and the core of dislocation in small angle GB in Fig. 6(c) provide 'rooms' to accommodate the segregated atoms. Figure 6(d) describes how the foreign Cu atoms are captured by local clusters in GBs through the two segregation mechanisms. Often, both segregation mechanisms occur simultaneously in the solute segregation processes.

Figure 7 presents the relative contributions of two mechanisms to total segregation of above four GBs. As shown in Fig. 7(a), substitutional segregation

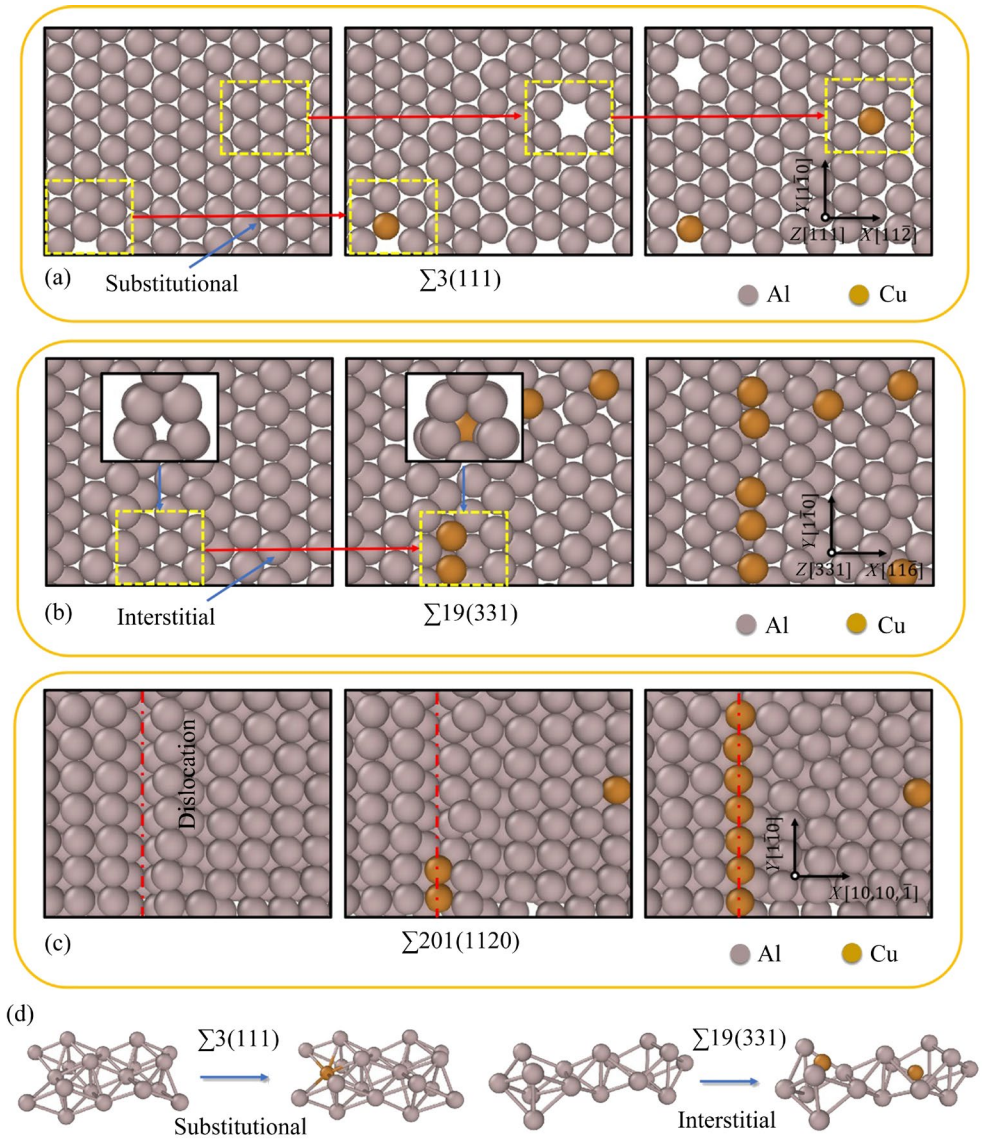

Fig. 6 Atomic scale segregation mechanism of GBs Σ3(111) (a), Σ19(331) (b) (The inset images represent the view along the [110] crystal direction), and Σ201(1120) (c); Schematic diagram of segregation mechanisms for structural units from twin GB Σ3(111) and GB Σ19(331) (d)

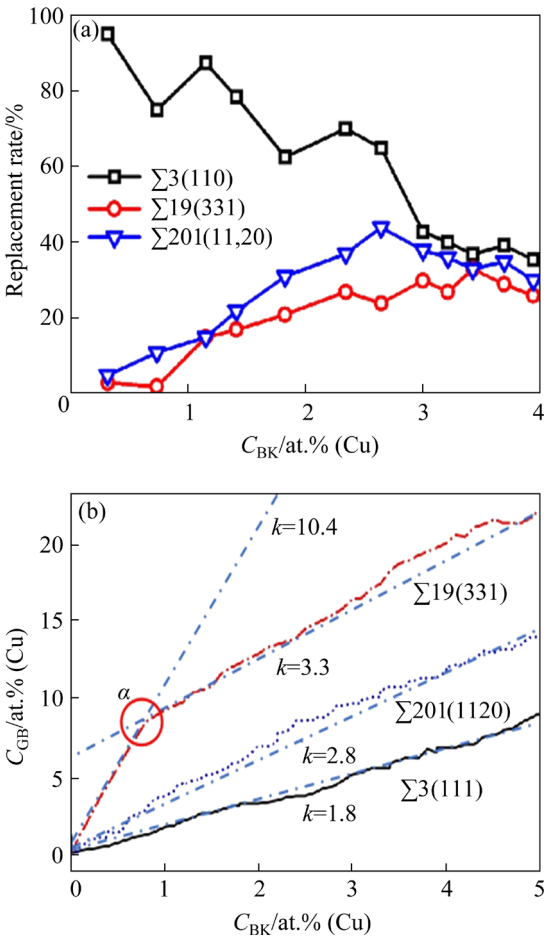

Fig. 7 Quantification of segregation kinetics affected by segregation mechanisms: (a) Contribution of substitutional segregation; (b) GBs concentration vs bulk phase concentration (C_{BK})

is dominant for solute segregation in the twin GB, but its weight decreases with Cu concentration in GBs. The substitutional segregation in the twin GB may lead to local strains around the segregated atoms, undermining the perfection of the lattice as the segregation level increases, as shown in Figs. 4(a) and 7(a). Then, the imperfect structures provide additional sites for interstitial segregation. Consequently, the weight for interstitial segregation increases as the segregation level increases. In contrast, when the interstitial sites in GBs are sufficient, the interstitial mechanism dominates significantly over the substitutional mechanism. However, as the interstitial sites are consumed by Cu atoms gradually, the substitutional mechanism becomes popular when such interstitial sites are exhausted, as exemplified by the segregation of the low-angle tilt GB, Σ201(11,20). In general, interstitial segregation is more prevalent because the GB is a relatively non-close packed structure with many imperfections.

The relationship between segregation level and grain bulk concentration is also studied. The dependence of the GB concentration (C_{GB}) on grain bulk concentration (C_{BK}) is quantified in Fig. 7(b). Here, segregation level k is defined as the ratio of C_{GB} to C_{BK}. Results show that twin GBs dominated by substitutional segregation exhibit lower segregation levels compared to normal high angle GB Σ19(331) dominated by interstitial segregation. The segregation level of the small angle GB Σ201(11,20) is higher than that of the twin GB due to the interstitial segregation at the cores of intergranular dislocations. The normal high angle GB Σ19(331) presents a complex variation of segregation level with the concentrations of grain bulk. The interstitial segregation mechanism dominates when the concentration of the bulk phase is less than 0.7%. This leads to a very high level of segregation, being about 10.4 which is nearly 6 times higher than that at k=1.8 of the twin GB dominated by substitutional segregation. However, as the sites for interstitial segregation are consumed gradually, substitutional segregation emerges and its weight increases gradually, and the segregation level decreases to about 3.3, much smaller than the segregation level for interstitial segregation. The results indicate that the segregation level is profoundly affected by the relative weight of the segregation mechanisms.

4 Conclusions

(1) The segregated atoms could profoundly affect GB structure. GB structures are prone to be undermined by segregated atoms. As the amount of segregated atoms increases, it is quantified that the order of GB structure decreases and converges gradually. In addition, the GB with a higher structure order is more susceptible to being undermined by segregated atoms.

(2) Two segregation mechanisms are found, namely the substitutional and interstitial segregation in different GBs. Both mechanisms work together on GB segregation but with different weights. The popularity of intergranular defects is conductive to the prevalence of interstitial mechanism, while substitutional mechanism is favored by the GBs with the highly ordered twin GB.

(3) The correlation among the level of GB segregation, segregation mechanisms and GB structure are illustrated. Structure order analysis demonstrates that interstitial atoms are more harmful to GB structure order than substitutional ones. Also, it is quantified that the GBs segregation dominated by interstitial mechanism tends to lead to a much higher level (up to about 6 times) than by substitutional mechanism.

CRediT authorship contribution statement

Xiong SHUAI: Data curation, Investigation, Writing – Original draft; **Hong MAO:** Data curation, Investigation; **Sai TANG:** Visualization, Writing – Original draft, Funding acquisition; **Yi KONG:** Supervision, Project administration; **Yong DU:** Supervision.

Declaration of competing interest

The authors declare that they have no known competing financial interests or personal relationships that could have appeared to influence the work reported in this paper.

Acknowledgments

This work was supported by grants from the National Natural Science Foundation of China (Nos. 52031017, 51801237), and the National Key Laboratory of Science and Technology on High-strength Structural Materials in Central South University, China (No. 6142912200106). We are grateful for technical support from the High-Performance Computing Center of Central South University, China.

Data Availability

The data that support the findings of this study are available from the corresponding authors upon reasonable request.

References

[1] LEJČEK P. Grain boundary segregation in metals [M]. Germany: Springer, 2010.

[2] KLIE R F, BUBAN J P, VARELA M, FRANCESCHETTI A, JOOSS C, ZHU Y, BROWNING N D, PANTELIDES S T, PENNYCOOK S J. Enhanced current transport at grain boundaries in high-T_c superconductors [J]. Nature, 2005, 435: 475−478.

[3] CHEN Y S, LU H Z, LIANG J T, ROSENTHAL A, LIU H W, SNEDDON G, MCCARROLL I, ZHAO Z Z, LI Wei, GUO A M. Observation of hydrogen trapping at dislocations, grain boundaries, and precipitates [J]. Science, 2020, 367: 171−175.

[4] PENG Z R, MEINERS T, LU Y, LIEBSCHER C H, KOSTKA A, RAABE D, GAULT B. Quantitative analysis of grain boundary diffusion, segregation and precipitation at a sub-nanometer scale [J]. Acta Materialia, 2022, 225: 117522.

[5] ZHOU X Y, KAMACHALI R D, BOYCE Brad L, CLARK B G, RAABE D, THOMPSON G B. Spinodal decomposition in nanocrystalline alloys [J]. Acta Materialia, 2021, 215: 117054.

[6] MA Z M, ZHANG Y , LIU S D, DENG Y L, ZHANG X M. Quenching sensitivity and heterogeneous precipitation behavior of AA7136 alloy [J].Transactions of Nonferrous Metals Society of China, 2021, 31: 3356−3369.

[7] WANG Q, LI Z, PANG S J, LI X N, DONG C, LIAW P K. Coherent precipitation and strengthening in compositionally complex alloys: A review [J]. Entropy, 2018, 20: 878.

[8] ZHOU L, WU C L, XIE P, NIU F J, MING W Q, DU K, CHEN JH. A hidden precipitation scenario of the θ'-phase in Al−Cu alloys [J]. Journal of Materials Science & Technology, 2021, 75: 126−138.

[9] RAABE D, SANDLÖBES S, MILLÁN J, PONGE D, ASSADI H, HERBIG M, CHOI P P. Segregation engineering enables nanoscale martensite to austenite phase transformation at grain boundaries: A pathway to ductile martensite [J]. Acta Materialia, 2013, 61: 6132−6152.

[10] RAABE D, HERBIG M, SANDLÖBES S, LI Y, TYTKO D, KUZMINA M, PONGE D, CHOI P P. Grain boundary segregation engineering in metallic alloys: A pathway to the design of interfaces [J]. Current Opinion in Solid State and Materials Science, 2014, 18: 253−261.

[11] ZHANG Y, JING H Y, XU L Y, HAN Y D, ZHAO L, LI H Z, TANG Z X, TONG T W. Microstructure and grain boundary engineering of a novel Fe−Cr−Ni alloy weldment made with self-developed composition-matched weld filler metal [J]. Transactions of Nonferrous Metals Society of China, 2020, 30: 992−1004.

[12] HAY R S, FAIR G E., KELLER K A, TIDBALL T, SUVACI E. Determination of 3-D alumina grain orientation, size, shape, and growth kinetics from 2-D data in Nextel™ 610 fibers [J]. Journal of the American Ceramic Society, 2015, 98: 2295−2306.

[13] LEJČEK P, VŠIANSKÁ M, ŠOB M. Recent trends and open questions in grain boundary segregation [J]. Journal of Materials Research, 2018, 33: 2647−2660.

[14] LI L L, KAMACHALI R D, LI Z M, ZHANG Z F. Grain boundary energy effect on grain boundary segregation in an equiatomic high-entropy alloy [J]. Physical Review Materials, 2020, 4: 053603.

[15] YANG W Q, MIN X, LIANG J X, YE M, ZHENG L. Non-equilibrium grain-boundary segregation of Bi in Cu bicrystals [J]. Transactions of Nonferrous Metals Society of China, 2014, 24: 4038−4043.

[16] SHUAI X, WANG Z J, MAO H, TANG S, KONG Yi, DU Y. Atomic-scale study of compositional and structural evolution of early-stage grain boundary precipitation in Al−Cu alloys through phase-field crystal simulation [J]. Journal of Materials Science, 2021, 56: 12700−12715.

[17] ZHOU X, YU XX, KAUB T, MARTENS R L, THOMPSON

G. B. Grain boundary specific segregation in nanocrystalline Fe(Cr) [J]. Scitific Report, 2016, 6: 34642.

[18] BACKHAUS-RICOULT M. Gibbs' adsorption at α alumina−copper interfaces [J]. Journal of the European Ceramic Society, 2003, 23: 2747−2759.

[19] KRAUß T, EICH S M. Development of a segregation model beyond McLean based on atomistic simulations [J]. Acta Materialia, 2020, 187: 73−83.

[20] BOKSTEIN B. S., SMIRNOV A N. Grain boundary segregation in Cu−Sb alloys [J]. Materials Letters, 2003, 57: 4501−4504.

[21] CUI Y, Chew H B. Machine-learning prediction of atomistic stress along grain [J]. Acta Materialia, 2022, 222: 117387.

[22] LUO Ting, MANGELINCK D, SERRANO-SÁNCHEZ F, FU Chen-guang, FELSER C, GAULT B. Grain boundary in NbCo (Pt) Sn half-Heusler compounds: Segregation and solute drag on grain boundary migration [J]. Acta Materialia, 2022, 226: 117604.

[23] PRITHIV T S, KLOENNE Z, LI Dian, SHI Rong-pei, ZHENG Yu-feng, FRASER H L, GAULT B, ANTONOV S. Grain boundary segregation and its implications regarding the formation of the grain boundary α phase in the metastable β-titanium Ti−5Al−5Mo−5V−3Cr alloy [J]. Scripta Materialia, 2022, 207: 114320.

[24] EBNER A S, JAKOB S, CLEMENS H, PIPPAN R, MAIER-KIENER V, HE Shuang, ECKER W, SCHEIBER D, RAZUMOVSKIY V I. Grain boundary segregation in Ni-base alloys: A combined atom probe tomography and first principles study [J]. Acta materialia, 2021, 221: 117354.

[25] MCKENZIE M E., MAURO J C. Hybrid Monte Carlo technique for modeling of crystal nucleation and application to lithium disilicate glass-ceramics [J]. Computational Materials Science, 2018, 149: 202−207.

[26] NAGAOKA M, SUZUKI Y, OKAMOTO T, TAKENAKA N. A hybrid MC/MD reaction method with rare event-driving mechanism: Atomistic realization of 2-chlorobutane racemization process in DMF solution [J]. Chemical Physics Letters, 2013, 583: 80−86.

[27] PLIMPTON S. Fast parallel algorithms for short-range molecular dynamics [J]. Journal of computational physics, 1995, 117: 1−19.

[28] LIU X Y, LIU C L, BORUCKI L J. A new investigation of copper's role in enhancing Al−Cu interconnect electro-migration resistance from an atomistic view [J]. Acta Materialia, 1999, 47: 3227−3231.

[29] PAN Z L, RUPERT T J. Formation of ordered and disordered interfacial films in immiscible metal alloys [J]. Scripta Materialia, 2017, 130: 91−95.

[30] SADIGH B, ERHART P, STUKOWSKI A, CARO A, MARTINEZ E, ZEPEDA-RUIZ L. Scalable parallel Monte Carlo algorithm for atomistic simulations of precipitation in alloys [J]. Physical Review B, 2012, 85: 184203.

[31] ATOMSK H P. A tool for manipulating and converting atomic data files [J]. Computer Physics Communications, 2015, 197: 212−219.

[32] STUKOWSKI A. Visualization and analysis of atomistic simulation data with OVITO−The open visualization tool [J]. Modelling and Simulation in Materials Science and Engineering, 2009, 18: 015012.

[33] SU S S, TANG S, LIANG C P, MA Y Z, LIU W S. Phase-field crystal study on the influence of nanoscale intergranular structures on grain boundary segregation [J]. Modelling and Simulation in Materials Science and Engineering, 2021, 29: 085009.

[34] OTSUKI A, MIZUNO M. Grain boundary energy and liquid metal embrittlement of aluminium [J]. Transactions of the Japan Institute of Metals, Supplement, 1986, 27: 789−796.

[35] CHANDRA N, DANG P Atomistic simulation of grain boundary sliding and migration [J]. Journal of Materials Science, 1999, 34: 655−666.

[36] UESUGI T, HIGASHI K. First-principles calculation of grain boundary energy and grain boundary excess free volume in aluminum: Role of grain boundary elastic energy [J]. Journal of Materials Science, 2011, 46: 4199−4205.

[37] PAIDAR V. A classification of symmetrical grain boundaries [J]. Acta Metallurgica, 1987, 35: 2035−2048.

[38] HERBIG M, RAABE D, LI Y J, CHOI P, ZAEFFERER S, GOTO S. Atomic-scale quantification of grain boundary segregation in nanocrystalline material [J]. Physical Review Letters, 2014, 112: 126103.

[39] KE X, YE J C, PAN Z L, GENG J, BESSER M F, QU D X, CARO A, MARIAN J, OTT R T, WANG Y M, SANSOZ F. Ideal maximum strengths and defect-induced softening in nanocrystalline-nanotwinned metals [J]. Nature Materials, 2019, 18: 1207−1214.

[40] PAN Z L, BOROVIKOV V, MENDELEV M I, SANSOZ F. Development of a semi-empirical potential for simulation of Ni solute segregation into grain boundaries in Ag [J]. Modelling and Simulation in Materials Science and Engineering, 2018, 26: 075004.

[41] KE X, SANSOZ F. Segregation-affected yielding and stability in nanotwinned silver by microalloying [J]. Physical Review Materials, 2017, 1: 063604.

[42] SANSOZ F, KE Xing. Hall−Petch strengthening limit through partially active segregation in nanocrystalline Ag−Cu alloys [J]. Acta Materialia, 2022, 225: 117560.

[43] MAHATA A, MUKHOPADHYAY T, ASLE ZAEEM M. Modified embedded-atom method interatomic potentials for Al−Cu, Al−Fe and Al−Ni binary alloys: From room temperature to melting point [J]. Computational Materials Science, 2022, 201: 110902.

[44] STEINHARDT P J, NELSON D R, RONCHETTI M. Bond-orientational order in liquids and glasses [J]. Physical Review B, 1983, 28: 784−805.

[45] LECHNER W, DELLAGO C. Accurate determination of crystal structures based on averaged local bond order parameters [J]. The Journal of Chemical Physics, 2008, 129: 114707.

[46] TANG S, WANG J C, SVENDSEN B, RAABE D. Competitive bcc and fcc crystal nucleation from non-equilibrium liquids studied by phase-field crystal simulation [J]. Acta Materialia, 2017, 139: 196−204.

铝铜合金晶界偏析微观机理的原子尺度研究

帅 熊[1]，毛 鸿[2]，唐 赛[3]，孔 毅[1]，杜 勇[1]

1. 中南大学 粉末冶金国家重点实验室，长沙 410083；
2. 湖南理工学院 机械工程学院，岳阳 414006；
3. 中南大学 轻质高强结构材料国家级重点实验室，长沙 410083

摘 要：通过采用分子动力学/蒙特卡洛联合模拟方法模拟铝铜合金中的过剩溶质原子在晶界的偏析过程，从而揭示晶界偏析的原子尺度微观机理。研究发现，晶界偏析过程中存在置换偏析和间隙偏析两种原子迁移机制。间隙偏析主要发生在晶界缺陷如位错、台阶面、空位和结构单元的空隙中；而置换偏析主要发生在具有较高有序度的孪晶界中。两种偏析机制对晶界结构的影响完全不同，间隙机制对晶界结构的破环性小于置换机制，并能够形成比后者更高(可达 6 倍)的溶质偏析程度。研究结果揭示了过量的溶质原子被吸附到晶界的原子尺度微观机理，并阐明了晶间结构、晶界偏析机理和偏析动力学之间的内在联系。

关键词：晶界偏析；铝铜合金；晶间结构；分子动力学模拟；蒙特卡洛模拟

(Edited by Bing YANG)